Probabilistic lithofacies prediction from prestack seismic data in a heterogeneous carbonate reservoir

Luanxiao Zhao[1], Jianhua Geng[2], Jiubing Cheng[2], De-hua Han[3], and Tonglou Guo[4]

ABSTRACT

We mapped probabilities of lithology and fluid based on seismic and well observations in a heterogeneous carbonate reservoir of the Sichuan Basin, southwest China, thus characterizing the reservoir complexity and identifying the potential sweet spot. Rock physical analysis showed that the presence of a vuggy-fracture porosity system combined with the fluids' effect complicate the elastic responses of heterogeneous carbonates. This also gives physical insight into how the elastic properties of different lithofluid classes can be distinguished. With the application of Bayesian linearized amplitude variation with offset inversion, we found that the posterior distribution of P- and S-wave velocities were reliably extracted, whereas the inverted density tended to show high uncertainty due to a lack of wide angle data in the migrated seismic gathers. Finally, a Bayesian approach was implemented to propagate uncertainty from prestack seismic data to lithofluid classes in an integrated framework. The gas-carbonate predictions with high posterior probabilities were consistent with well observations at the well location and the present geological continuity. The probability distributions for the anhydrite, limestone, and dolostone were essential to understand the reservoir architecture and delineate the reservoir heterogeneities. We also ascertained that the uncertainty of lithofacies prediction is determined by the uncertainty of seismic inversion as well as the uncertainty of the link between lithofacies to their corresponding elastic responses.

INTRODUCTION

Seismic characterization of carbonate reservoirs is challenging. This is mainly because carbonates constantly undergo physical, chemical, and biological changes during sedimentation and postdepositional diagenesis, thereby causing significant heterogeneities in rock properties. Quantitative lithofacies delineation from seismic data is considered to be an important tool for understanding such complexities and heterogeneities in carbonate reservoir. In this article, we present a case study to show how to predict probability distributions of lithology and fluid from prestack seismic data in a Paleozoic marine carbonate reservoir, Sichuan Basin, southwest China. This geologically complex carbonate reservoir exhibits the characteristics of very deep burial depth, overmatured source rock, and strong heterogeneities due to the extensive diagenesis in geologic history (Ma et al., 2008b).

Many factors can cause uncertainties for lithofacies prediction from seismic data, such as data noise from geophysical measurements and processing, approximation of physical models and also the associated scale changes (Mukerji et al., 2001; Houck, 2002; Avseth et al., 2005; Grana and Rossa, 2010). This is especially true for carbonate reservoirs, which display wide variations in rock properties due to the complicated geologic processes. From the statistical point of view, such uncertainties can be reduced if more disparate sources of data, such as geologic knowledge, seismic data, rock physics, and core information, can be combined. A Bayesian setting will be a natural choice to integrate all the available information to characterize the inversion uncertainty (Tarantola, 1987; Eidsvik et al., 2004; Gunning and Glinsky, 2007; Bosch et al., 2010). In general, probabilistic lithology and fluid prediction from prestack seismic data entails the uncertainty of seismic inversion and rock-physics inversion, and it has been studied by many authors

through proposed methodologies and case studies (Eidsvik et al., 2004; Larsen et al., 2006; Buland et al., 2008; González et al., 2008; Rimstand and Omre, 2010; Ulvmoen and Omre, 2010; Rimstad et al., 2012). However, most of those studies focus on sandstone reservoirs with relatively less heterogeneities, and it is still very challenging to demonstrate its application in the studied carbonate reservoirs, which present strong heterogeneities. This is mainly due to two factors described in the following two paragraphs.

First, the burial depth of the studied carbonate reservoir is deeper than 6 km, and hence the signal-to-noise ratio (S/N) in the seismic data is reduced significantly. Also, the deep targeted reservoir makes it hard to obtain wide-angle gathers, resulting in difficulties to extract reliable elastic parameters (P-wave velocity, S-wave velocity, and density) through seismic inversion. To reveal the reliability of the seismic inversion results for further quantitative lithology prediction, it is necessary to evaluate their associated uncertainties. In this study, we perform amplitude variation with offset (AVO) inversion in the Bayesian framework to estimate the posterior distribution of the inverted elastic parameters (Buland and Omre, 2003).

Second, the complex diagenesis complicates the rock-physics relationship in carbonates, which in turn makes seismic response poorly understood. Therefore, understanding the sensitivity of the elastic properties of carbonates to the fluids' effect is critical to test the feasibility of lithology and fluid prediction from seismic attributes. The elastic responses in carbonates are often considered to be less sensitive to the fluids' effect because carbonate rocks are often very stiff. However, the fluids' effect on the seismic rock properties of carbonates can be dramatically amplified due to the presence of heterogeneities and fractures (Li et al., 2003; Han, 2004). Rock-physics modeling is used to study how the elastic properties of different lithofluid classes in this heterogeneous carbonate reservoir can be distinguished, thereby providing physical insights into lithology and fluid prediction from seismic data.

The intent of this paper is not to focus on the details of the probabilistic inversion methodologies. Rather, through a case study, our goal is to investigate how the geologic understanding and rock-physics analysis can help us better understand and constrain the lithofacies prediction from seismic data in a probabilistic framework. The paper is structured as follows: We first introduce the geologic background and related data set in the carbonate reservoir of the Sichuan Basin, southwest China. The categorical lithology and pore-fluid scenarios, which are termed as lithofacies classes, are defined based on geologic information and well-log analysis prior to the inversion. We then use rock-physics modeling to physically link the defined lithofluid classes to the elastic properties. Next, a fast Bayesian simultaneous AVO inversion approach is performed to estimate elastic properties and their associated uncertainties in a 2D inline section extracted from a 3D migrated seismic data set. Finally, we present and analyze the probabilistic lithology and fluid inversion results from this 2D seismic data set.

GEOLOGIC SETTING AND DATA DESCRIPTION

The studied Yuanba gas field is the deepest marine strata gas field found in China, and it is located in the northern end of the gently deformed structural belts in the central Sichuan Basin (Long et al., 2011). The reservoir rocks in the Lower Triassic formation are primarily controlled by the oolitic shoal facies developed on the evaporitic carbonate platform edge. The evaporate beds of the lagoon-tidal flat facies in the Lower and Middle Triassic strata formed the cap rock for the underlying gas accumulations (Ma et al., 2008b). The deep buried reservoirs suffer multiphase tectonic movements after deposition, which make the secondary diagenetic processes very complex and thereby strongly reorganize the pore space of reservoir rocks. The main diagenetic processes include compaction-pressure solution, selective dissolution, fracturing, dolomitization, and recrystallization.

A stacked image of the seismic data is shown in Figure 1, in which the red vertical line indicates the location of the available well. The structures within the targeted seismic inversion zone appear relatively flat. For the purpose of AVO inversion, the seismic data have been processed by a processing contractor with an amplitude-preserving workflow, ensuring that prestack data represent the true offset dependent reflectivity. The quality of the seismic data can be characterized as good with an S/N of around four.

Well logs play an important role in linking rock properties to seismic data, which should be extensively analyzed prior to the lithofacies inversion. The well-log data of lithology content, P-wave velocity, S-wave velocity, density, and water saturation after depth-to-time conversion, are displayed as functions of two-way traveltime in Figure 2. As we can see from the curve of the water saturation, gas-saturated dolostones are trapped between the layers of brine saturated dolostone from the depth of 2680 to 2730 ms. Here, dolomitization is considered to play a large role in improving reservoir quality through increasing particle size in the mud-dominated fabrics by replacing the lime mud with medium-size dolomite crystals (Lucia, 1999). In addition, dolostone is less compactable and hence more favorable for porosity preservation. There are several layers of anhydrite deposition, which are attributed to the frequent sea-level fluctuations. The occurrence of anhydrite is often linked to diagenetic processes of evaporite mineralization. Note that the overburden anhydrite that ranges from 2650 to 2680 ms, which is considered the seal for the underlying dolostone reservoir, contains some thin shale and dolostone layers. The well-log also shows a thick limestone formation that is controlled by a relatively stable depositional environment. More shale content is found in this limestone unit, which is often associated with the low energy depositional environment, possibly in a lagoonal or central platform setting. Nonetheless, the dolostone reservoir is pretty clean, which
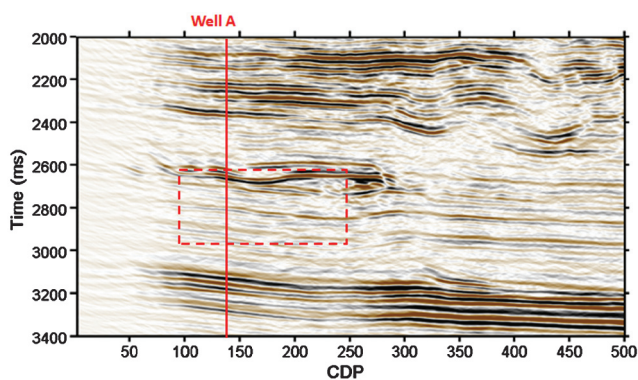

Figure 1. Stacked seismic image of inline 209 (the negative amplitudes are red, and the positive amplitudes are black). The dashed rectangle identifies the targeted inversion zone, and the red line identifies the position of well A.

suggests that the depositional environment is probably related to the higher energy setting such as platform margins. Based on the geologic knowledge and petrophysical interpretation of well-log data, we define four lithofacies in the targeted inversion zone: anhydrite, dolostone, gas-carbonates, and limestone. The lithofacies show fairly strong vertical variations based on this single well analysis, implying that the reservoir exhibits complex depositional and diagenesis in the geologic history. Rock properties can also be discerned from well-log data. For example, the trapped gas-carbonates present elastic features of low velocity and low density. Further-

more, dolostone generally has higher P- and S-wave velocities, whereas anhydrite tends to have higher density.

ROCK-PHYSICS ANALYSIS

The prediction ability is strongly dependent on the degree of separation for lithofacies given seismic-derived elastic properties. Statistical rock-physics relationships that are derived from well-log data represent the link between the lithofacies to their corresponding elastic properties. More importantly, it is critical to understand
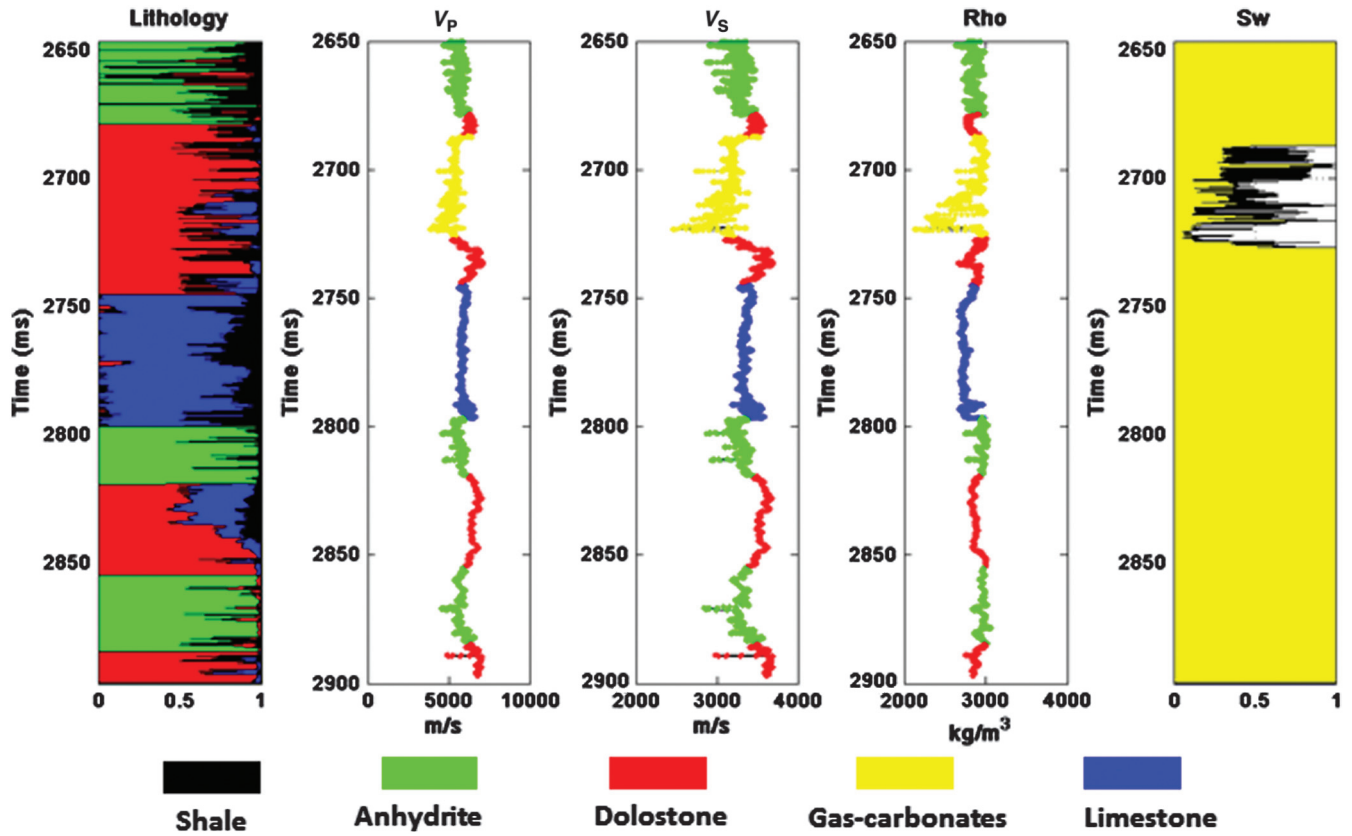

Figure 2. P-wave velocity, S-wave velocity, density, and water saturation are displayed as a function of two-way traveltime in well A. Litho-fluid classes are defined. Green, red, yellow, and blue represent lithofacies of anhydrite, dolostone, gas-carbonates, and limestone, respectively.

Figure 3. Core photos of reservoir rocks in the Yuanba gas field of Sichuan Basin, southwest China. Red parts represent pore space. (a) Fine-medium crystal dolomitic limestone with microfractures, (b) power crystal dolostone with vuggy pores and microfracture, and (c) power crystal dolostone with vuggy pores and microfractures.

why the inverted elastic attributes can physically be used to identify the lithofluid classes based on the geologic understanding of this reservoir. In this section, we perform rock-physics analysis to demonstrate how the heterogeneities of rock properties affect the resulting elastic responses.

Vuggy-fracture porosity system

Geologic observations suggest that the diagenetic product of fracturing, dissolution, compaction, and dolomitization significantly improve the deep-buried reservoir quality. The pore space is hence dominated by the secondary porosity. Figure 3 shows core plugs representative of the carbonate reservoir formation in the Sichuan Basin. The heterogeneous pore systems are closely related to small-scale touching vugs (grain molds) and microfractures. Typically, most of the fluid storage is in the vuggy system and most of the flow capacity is in microfractures.

Vugs or moldic porosities are often formed from dissolution processes by selectively dissolving grains composed of unstable minerals. Such dissolution processes can occur within the meteoric environment associated with fresh water or in the burial environment (Lucia, 1999). Moreover, the rich sour gas, such as H_2S in this reservoir, is believed to enhance the dissolution effect. Normally, the vugs, or grain molds are often isolated and have poor connectivity. Fortunately, the well-developed microfractures increase the connection between the separate vugs and enhance the permeability dramatically. This is supported by the fact that the reservoir rocks have an average porosity of about 4%–5%, but the effective permeability could be as high as several hundred millidarcies based on the core measurements. Microfractures in this reservoir could be associated with dolostone's brittleness and differential stress due to the multiphase tectonic movement. Additionally, the developed microfractures, which serve as fluid conduits, are favorable for dissolution to take place. Overpressure is another important factor that should be considered to facilitate the development and preservation of the secondary porosity. First, overpressure can increase the solubility of acid gas (CO_2 and H_2S), and it thereby enhances the dissolution ability of formation water. Second, overpressure tends to preserve vuggy-fracture porosity system during the process of burial compaction (Ma et al., 2008a).

Rock-physics modeling

Rock physics modeling is used to learn how the vuggy-fracture porosity system and fluid behavior together affect the elastic properties. The dry-rock elastic moduli are computed using the differential effective medium theory (Mavko et al., 2009; Xu and Payne, 2009; Zhao et al., 2013). This scheme simulates porosities in a composite of two phases by incrementally adding a small amount of pores (phase 2) into a matrix (phase 1). The coupled system of ordinary differential equation can then be written as

$$(1 - \phi)\frac{d}{\phi}[K^*(\phi)] = (K_2 - K^*)P^{(*2)}(\phi), \qquad (1)$$

$$(1 - \phi)\frac{d}{\phi}[\mu^*(\phi)] = (\mu_2 - \mu^*)Q^{(*2)}(\phi). \qquad (2)$$

With the initial conditions $K^*(0) = K_1$ and $\mu^*(0) = \mu_1$, where K_1 and μ_1 are the matrix bulk and shear moduli, respectively;

K_2 and μ_2 are the bulk and shear moduli of the inclusion phase, respectively; φ is the porosity and $d\varphi$ is the incremental change in porosity; and $P^{(*2)}$ and $Q^{(*2)}$ are the geometric factors depending on the aspect ratios of the elliptical pores. In this case, the pore space is assumed to consist of a combination of stiff matrix porosity (vuggy pores) and microfractures with aspect ratios of 0.4 and 0.01, respectively. The solid matrix is assumed to be dolomite based, the matrix porosity is assumed to be 0.05, and the crack density varies from 0 to 0.30, which is calculated from the crack-induced porosity and the aspect ratio of the cracks (Hudson, 1981). The gas-brine carbonate reservoir is assumed to be partially saturated, and the effective fluid modulus is computed based on the Voigt average approximation (Domenico, 1976; Mavko et al., 2009):

$$K_f = S_w K_w + S_g K_g, \qquad (3)$$

where K_f is the effective bulk modulus of the fluid mixture; K_w and K_g, respectively, denote the bulk moduli of the brine and gas phases; and S_w and S_g, respectively, denote the water saturation and gas saturation. Finally, Gassmann's fluid substitution method is performed to add the fluid mixture to obtain the elastic response of the saturated rock.

The simulated elastic properties of the carbonate's V_P/V_S ratio versus P-impedance superimposed with well-log data are displayed in Figure 4. The rock-physics modeling result explains the scattering point in terms of fluids and porosity heterogeneities. Figure 4a and 4b mainly illustrates the effect of crack density and water saturation, respectively. It turns out that the vuggy-fracture porosity system combined with the fluids' effect complicate the elastic responses of the heterogeneous carbonates. They show that the gas has a strong effect on reducing P-impedance and V_P/V_S ratio for fractured carbonates, and this effect becomes stronger with higher crack density. However, the brine-saturated fractured carbonates exhibit slight increase in V_P/V_S ratio and slight decrease in P-impedance for intensely fractured carbonates. Physically, when the fractures are dry or filled with gas, the seismic propagation velocity that is normal to the fracture will be significantly decreased. In contrast, the brine drastically stiffens the very compliant fractures (Schoenberg and Sayers, 1995). Consequently, it is physically reasonable to understand that gas-carbonates in this reservoir can have a good separation with the other three lithofacies. Figure 4b shows that well-log data from the gas-carbonate interval nicely comply with the different water saturation lines. It seems to be hard to separate the saturation effect at low crack density (<0.10), but the separation becomes significant with increasing crack density. Generally, the carbonate reservoir rocks having high gas saturation are often associated with high crack density, implying that the prospective sweet spots potentially enjoy high effective permeability. In addition, Figure 4a also suggests that anhydrite, dolostone, and limestone can be distinguished to a certain degree. The spreads of those brine-saturated lithofacies are considered to be largely caused by the mineralogy effects based on the petrophysical interpretation of log data (Figure 3), and they may also reflect the variability of complex pore systems in the heterogeneous reservoir rocks. Note that some scatters of anhydrite overlap with gas-saturated dolostone and present a relatively lower V_P/V_S ratio (Figure 4a). This is possibly caused by a certain amount of gas leakage into the silty stringers or fractured zones within the overburden anhydrite layer.

PROBABILISTIC LITHOFACIES PREDICTION

In this section, we make inferences about the defined categorical lithofacies from prestack seismic data. The lithofacies $\mathbf{f}$ and seismic data $\mathbf{d}$ can be linked via a set of elastic parameters $\mathbf{m}$. In a Bayesian inversion setting, the posterior distribution for $\mathbf{f}$ given the seismic gather $\mathbf{d}$ is generally expressed as (Buland et al., 2008)

$$p(\mathbf{f}|\mathbf{d}) = \int \cdots \int p(\mathbf{f}|\mathbf{m})p(\mathbf{m}|\mathbf{d})d\mathbf{m}. \qquad (4)$$

Note that this equation only holds with the assumption of conditional independence $p(\mathbf{f}|\mathbf{m}, \mathbf{d}) = p(\mathbf{f}|\mathbf{m})$, which implies that the seismic data do not give any additional information for the lithofacies prediction when the elastic parameters are already known.
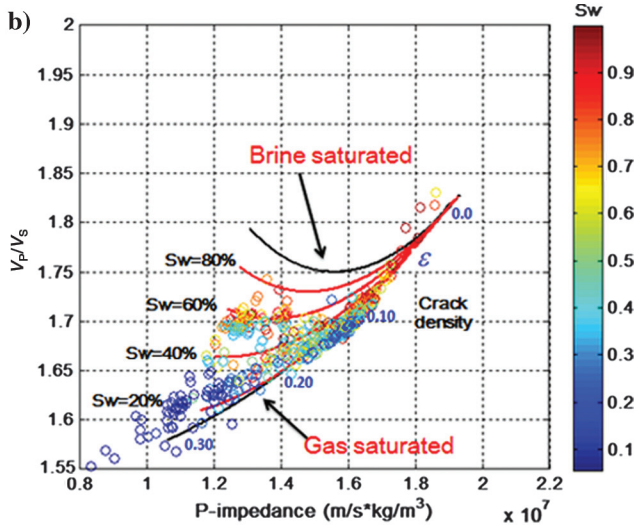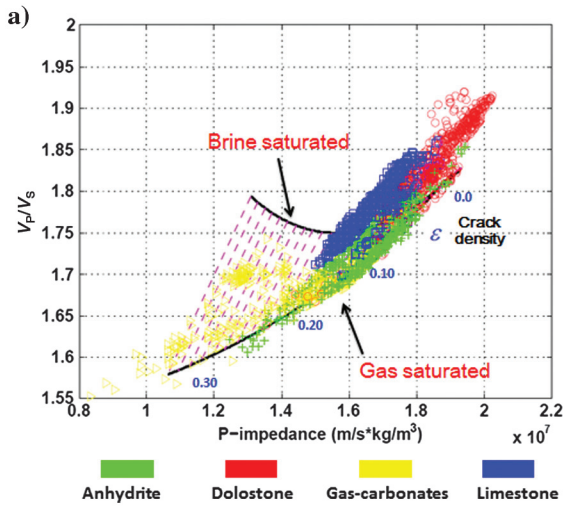

a)

b)

Figure 4. A rock-physics template presented as crossplots of V_P/V_S versus P-impedance, which is used to illustrate the effect of (a) crack density and (b) fluid saturation. The two black lines indicate 100% gas saturated and 100% brine saturated, the dashed pink lines in panel (a) represent modeling results with different crack densities, and the red solid lines in panel (b) indicate the impact of different fluid saturation. Scattering data points in panel (b) are only from the well-log data of gas carbonate interval, and they are color coded by water saturation.

It is clear to see that equation 4 propagates uncertainty from seismic data to lithofluid classes by integrating two posterior probabilities. The first is the posterior probability of elastic attributes given seismic data obtained by a Bayesian inversion approach (Buland and Omre, 2003). The second is the posterior probability of lithofacies conditioned by elastic attributes based on the rock-physics inversion.

Bayesian seismic inversion

According to Bayes' theorem, the posterior distribution of elastic parameters given seismic data $p(\mathbf{m}|\mathbf{d})$ in equation 4 is defined as

$$p(\mathbf{m}|\mathbf{d}) \propto p(\mathbf{d}|\mathbf{m})p(\mathbf{m}), \qquad (5)$$

where $p(\mathbf{d}|\mathbf{m})$ is the seismic likelihood function and $p(\mathbf{m})$ is the prior model for the elastic parameters. The seismic likelihood is defined by the convolutional model with discrete matrix formulation in Buland and Omre (2003) and Buland et al. (2008). The prior model $p(\mathbf{m})$ combines the contribution of the rock-physics likelihoods and prior probabilities for all the defined lithofacies:

$$p(\mathbf{m}) = \sum_{f=1}^{N} p(\mathbf{m}|\mathbf{f})p(\mathbf{f}), \qquad (6)$$

where $p(\mathbf{m}|\mathbf{f})$ is the rock-physics-likelihood function, $p(\mathbf{f})$ is the prior lithofacies model, and N is the total number of lithofacies. The rock-physics likelihood is simulated from statistical rock-physics analysis of the available log data in Well A. Because the prior geologic and spatial information about the lithofacies distribution in the targeted zone are not taken into account, the prior probabilities assigned to the each defined lithofacies classes are set as 0.25. Obviously, $p(\mathbf{m})$ has the multimodal distribution with each mode representing each lithofacies, which is mathematically inconveniently
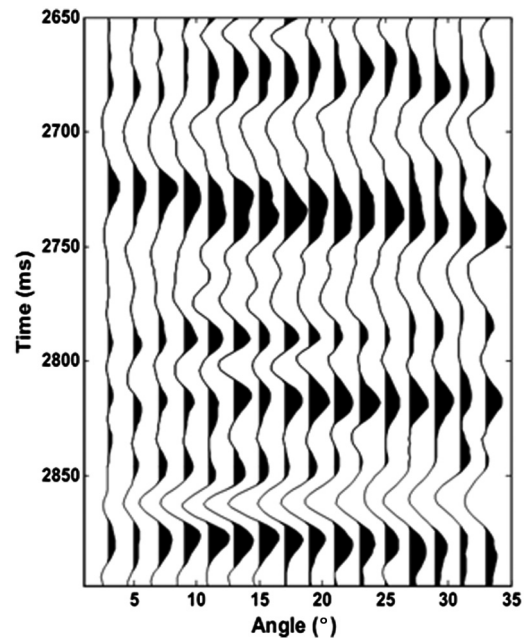

Figure 5. The angle gather at the well position, which is transformed from the offset-domain common-image gathers. The maximum incident angle obtained here is 33°.

used as a prior model for seismic inversion. Consequently, we approximate $p(\mathbf{m})$ to $p_*(\mathbf{m})$ with Gaussian distribution, which is characterized by the expectation vector, the covariance matrix, and the spatial-correlation function (Buland and Omre, 2003; Larsen et al., 2006; Buland et al., 2008).

To perform Bayesian amplitude variation with angle (AVA) inversion, we transform migrated prestack seismic gathers from the offset domain to the reflection angle domain. Figure 5 shows the transformed angle gather at the well position. Because the targeted
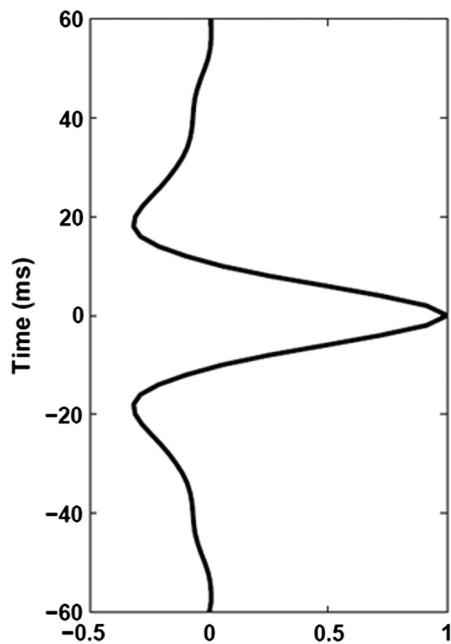

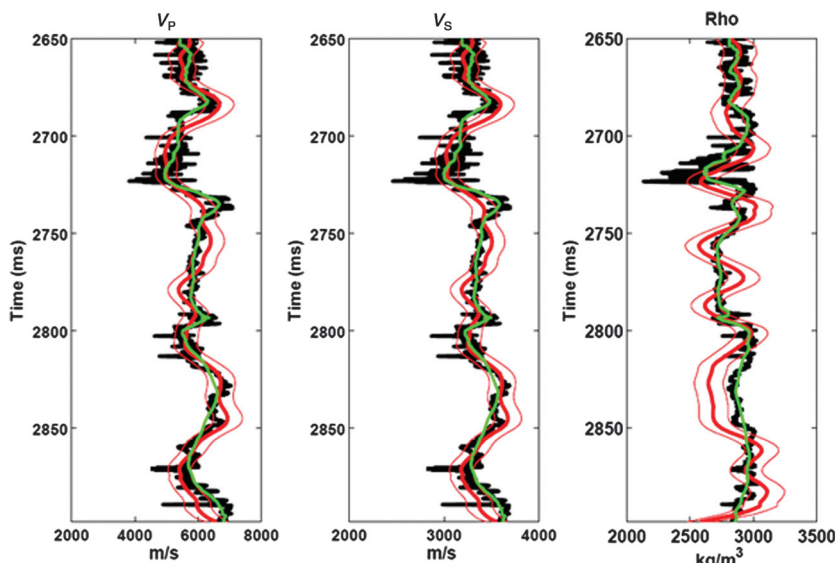Figure 6. The angle-independent wavelet used in the inversion.

Figure 7. Seismic inversion result at the well position. The black line indicates the actual well-log data, the green line indicates well-log trend, the red thick line indicates a maximum solution, and the red thin lines indicate an 0.9 prediction interval.

carbonate reservoir is very deep, the largest incident angle obtained is about 33°. The wavelet used in the inversion is extracted from seismic data in the well-tie setting, as shown in Figure 6. Note that the wavelet in this case is angle independent, which is mainly based on the fact that the prestack gathers have been preconditioned including offset and spectral balancing of the seismic amplitudes. To a certain degree, this can mitigate the impact of wavelet stretch and increase the fidelity of angle gathers for AVA inversion. However, to get more reliable inversion results, angle-dependent wavelets are required to correct for uncertainties due to anisotropy effects, overburden effects, attenuation effects, and so on. Moreover, the low-frequency information used to constrain seismic AVA inversion comes from the expectation of the prior model of elastic parameters, which assumes smoothing variations of elastic properties in the targeted inversion window. Nonetheless, for lithofacies having large contrasts and rapid variations of elastic properties, it is also reasonable to give separate prior models for different lithofacies to provide better discriminability of the low-frequency background trend.

The inversion results at the well position (Figure 7) show that the inverted P- and S-wave velocities fit well with the well-log trends, and some details of the vertical change can even be captured. However, the inverted density is not accurate enough to be retrieved. The 0.9 confidence intervals indicate that the uncertainty of the inverted density is much higher than that of the inverted P- or S-wave velocity. This is likely to be caused by the realistic noise levels of seismic data and lack of wide-angle reflectivity gather in the deep targeted formation. The maximum a posteriori solution within the targeted zone is shown in Figure 8. According to the previous rock-physics analysis, the very low acoustic impedance and V_p/V_s ratio from 2690 to 2740 ms in the seismic inversion result can be regarded as the potential gas reservoir. The next step is to map the probability of the gas carbonate reservoir.

Assessment of the posterior model

Following the approach presented in Buland et al. (2008), the approximate likelihood model for the seismic data given lithofacies can be written locally for the time sample i as

$$p(\mathbf{d}|f_i) \propto \iint \frac{p(\mathbf{m}_i|f_i)p_*(\mathbf{m}_i|d)}{p_*(\mathbf{m}_i)} d\mathbf{m}_i,$$

(7)

where $p_*(\mathbf{m}_i|\mathbf{d})$ is the posterior seismic inversion result using the Gaussian prior model $p_*(\mathbf{m}_i)$. Here, we do not use density information for reliable lithofacies prediction due to its poor inversion result as shown in Figure 7, even though it is an important input to constrain the lithofacies prediction, especially for the separation of gas carbonates. Thus, only P- and S-wave velocities are used as links to estimate lithofacies probabilities from seismic data. Recall that the relationship of P- and S-wave velocities in this heterogeneous carbonate reservoir exhibits significant variation due to the presence of the complex vuggy-fracture porosity system as well as the fluids' effect; therefore, we assume that the P- and S-wave velocities independently provide information to constrain

the lithofacies prediction. This entails the conditional independence between P- and S-wave velocities, and the rock-physics likelihood can be consequently expressed as

$$p(\mathbf{m}_i|f_i) = p(Vp_i|f_i)p(Vs_i|f_i). \quad (8)$$

The histograms of four lithofacies' P- and S-wave velocities in well A are shown in Figure 9a. The rock-physics likelihoods displayed in Figure 9b are assumed to follow the Gaussian distribution and can be calculated from the associated expectation and variances. As expected, the elastic properties of gas-carbonates can separate well with the other three lithofacies, but the variance and associated uncertainty tend to be higher. Also, the elastic properties of the anhydrite, limestone, and dolostone are overlapping each other to a certain degree, but they present relatively lower variance and associated uncertainty.

The approximate likelihood function in equation 7 and prior probabilities of lithofacies define the approximate posterior lithofacies distribution:

$$p(f_i|\mathbf{d}) \propto p(\mathbf{d}|f_i)p(f_i), \quad (9)$$
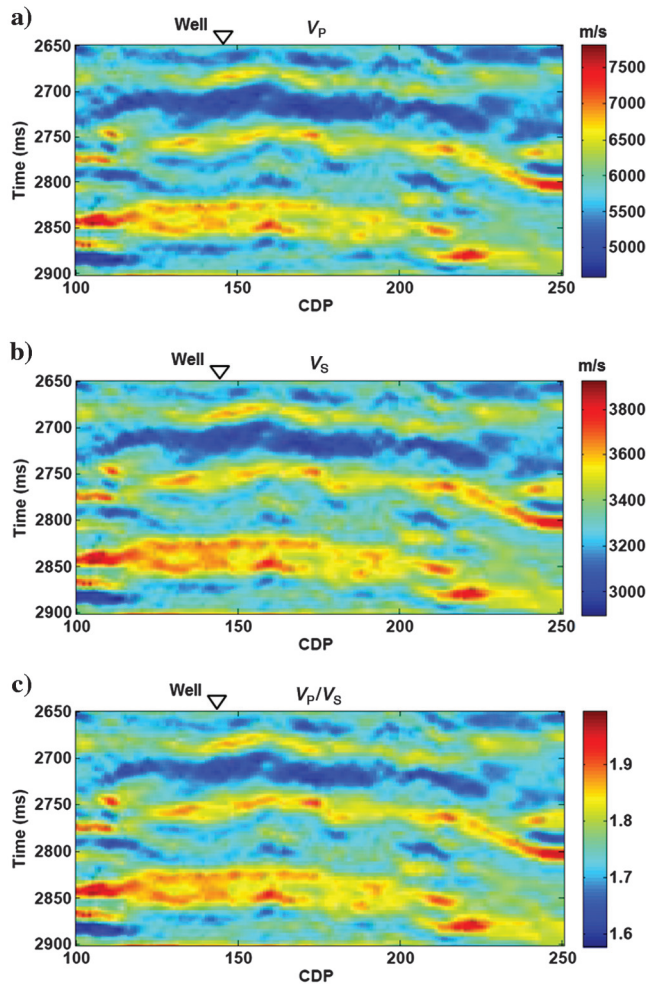
which can be normalized as

$$\sum_{f=1}^{N} p(f_i|\mathbf{d}) = 1. \quad (10)$$

To efficiently solve the integral in equation 7 (see Buland et al., 2008), the likelihood function $p(\mathbf{d}|f_i)$ can be considered as a convolution of the ratio $h(\mathbf{m}_i|f_i) = p(\mathbf{m}_i|f_i)/p_*(\mathbf{m}_i)$, with the Gaussian kernel $g(\mathbf{m}_i - \hat{\mathbf{m}}_i) = p_*(\mathbf{m}_i|\mathbf{d})$:

$$p(\mathbf{d}|f_i) = \iint h(\mathbf{m}_i|f_i)g(\mathbf{m}_i - \hat{\mathbf{m}}_i)d\mathbf{m}_i. \quad (11)$$

Here, $\hat{\mathbf{m}} = \mu_{m|d}$ represents the posterior expectation of Bayesian seismic inversion. Now, the convolution in equation 11 can be

Figure 8. Maximum a posteriori seismic inversion results of P-wave velocity, S-wave velocity, and V_P/V_S ratio within the targeted zone.
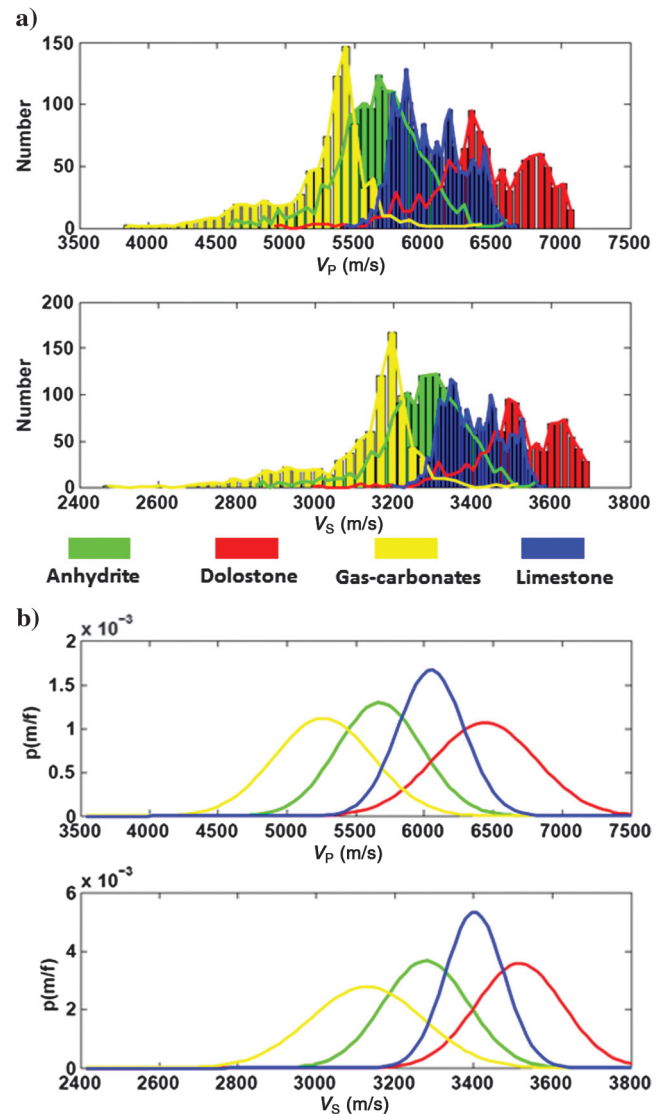

Figure 9. (a) Histograms for the four lithofacies' P- and S-wave velocities. The curves are used to plot the boundary of the histogram for each lithofacies. The data used are from the well log A in the targeted reservoir. The yellow, green, blue, and red colors represent the lithofluid classes of gas-carbonates, anhydrite, limestone, and dolostone, respectively. (b) The rock-physics likelihoods for the four lithofacies and the probability distributions for the P- and S-wave velocity are assumed to be Gaussian.

numerically realized in the Fourier domain by the use of fast Fourier transform. Consequently, we can compute the posterior probabilities of lithofacies by looking up the precalculated likelihood after Bayesian seismic inversion. In addition, we do not make any assumptions about spatial dependency of lithofacies in neighboring cells to assess the posterior model in this case study.

Results of the posterior probabilities for the lithofacies

Figure 10 displays the posterior probability for anhydrite, dolostone, gas-carbonates, and limestone at the well position. The sum of posterior probability of all lithofacies is equal to one. For a perfect prediction, the probability would be one in the position of reference lithofluid classes and zero otherwise. Generally, the predicted posterior probabilities for the lithofacies are acceptable compared with the actual lithology profile defined at the well position. It is observed that the probabilities of gas-carbonates occurrence at the reservoir zones (2700–2740 ms) are about 0.6–0.7, which demonstrates that the gas-carbonates are highly predictable. This is mainly due to two reasons: First, the inverted elastic properties from seismic data have a good match with the actual log data and the associated uncertainty is low in the gas-carbonate zone; second, the rock-physics relationships for the gas-carbonates have a good separation with other lithofacies. The prediction ability for the dolostone is high at depths ranging from 2690–2700 ms and 2820–2850 ms. However, it is reduced at depths ranging from 2740–2750 ms and 2890–2900 ms, where they are mistaken as limestone. A possible explanation for this may be attributed to the poor elastic property inversion results at the corresponding depths. Even though the rock properties of the dolostone, limestone, and anhydrite can be discriminated to a certain degree, errors occasionally occur for discriminating anhydrite, dolostone, and limestone.

The posterior probabilities of gas-carbonate, anhydrite, dolostone, and limestone for the targeted zone are displayed in Figures 11 and 12. The lithofacies profile from well A is also marked for easy comparison with the predicted result. The inversion result suggests that the gas carbonates in the top of the targeted zone (2700–2750 ms) show varying posterior probabilities ranging from 0.5 to 0.8. Although the inversion procedure goes trace by trace, without considering the lateral continuity, the predicted probabilities about the gas-carbonate area still show spatial continuity geologically. Also, the reservoir rocks tend to be heavily cracked based on the previous rock-physics analysis. In conjunction, those factors increase our confidence to identify the gas carbonate reservoir with high posterior probability as the potential sweet spots. We also map the posterior probabilities of anhydrite, dolostone, and limestone. The targeted zone shows significant heterogeneities in terms of the lithology distribution, which in turn gives feedback about the varying depositional environment and strong diagenesis that reorganized the reservoir in geologic history. Even though the prediction uncertainty may be high in certain areas, it is still useful for the delineation of the reservoir architecture and construction of the geologic model.
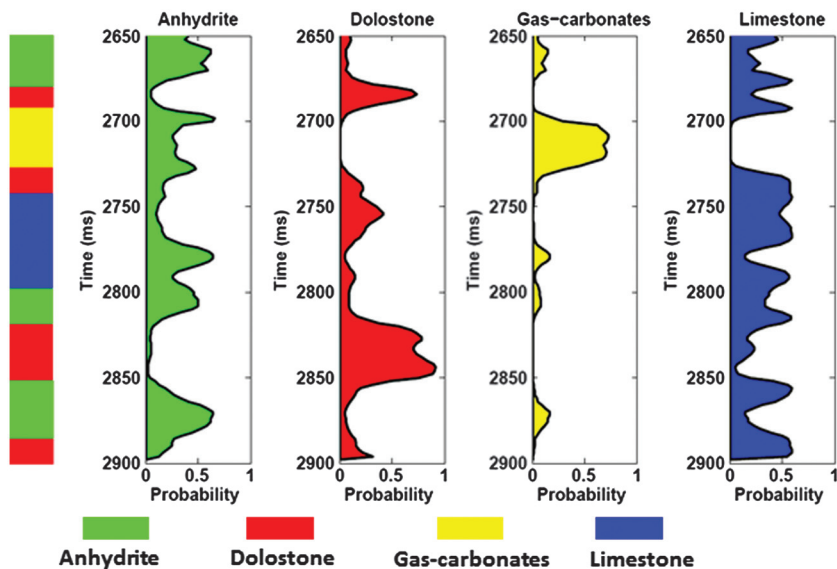

Figure 10. (Left) The reference lithology and fluid profile, with anhydrite (green), dolostone (red), gas-carbonates (yellow), and limestone (blue), is defined based on the well-log analysis. (Right) Posterior probabilities for lithofacies prediction from seismic data at the well position. The sum of posterior probability of each lithofacies is equal to 1.

DISCUSSION

The main limitation in this case study is that the prior information about the spatial correlation for the lithofacies model has not been taken into account. Generally, the prior model for the seismic lithofacies inversion can be constructed based on the available geologic information, well-log data, and seismic interpretation. Numerically, the prior model on the lithofacies
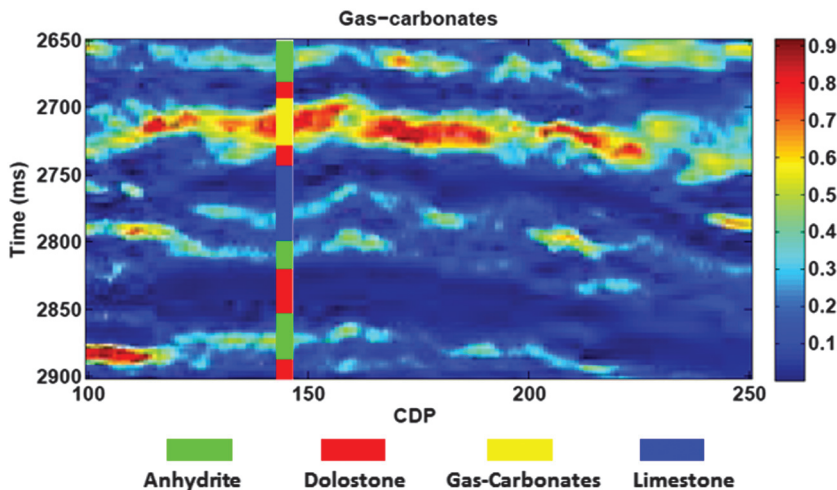

Figure 11. Posterior probability for gas-carbonate distributions in the targeted reservoir. The corresponding lithofacies profile from well A is plotted for comparison with the inversion results.

classes can be characterized by a Markov random field that captures the locally vertical and horizontal continuities (Eidsvik et al., 2004; Larsen et al., 2006; Rimstad and Omre, 2010; Ulvmoen and Omre, 2010). This should be considered in future work. Also, in this case, we only use P- and S-wave velocities to infer the lithofacies probabilities from seismic because the density is not reliably extracted based on the three-term AVO inversion. It is also practically possible to use the elastic attributes of P-impedance in combination with the V_P/V_S ratio, which can be readily estimated using two-term AVO information. This might enhance the prediction ability to distinguish gas-carbonate from anhydrite because they have less overlap if the information of P-impedance is included as illustrated in Figure 4a. In addition, we assume the conditional independence of P- and S-wave velocities in the rock-physics likelihood to predict posterior probabilities of lithofacies. Strictly speaking, this assumption is considered to be not in accordance with the seismic inversion result because there exist some dependencies for the P- and S-wave velocities inverted from the AVO attributes. It is important to note

that this should be considered as a special case for this heterogeneous carbonate reservoir where the presence of complex pore system and fluid saturation effect result in strong P- and S-wave velocity variations. However, such a treatment may subjectively enhance the prediction certainty because we do not account for the redundancy in the information of elastic parameters.

The rock-physics likelihood and the prior elastic model used for seismic inversion are better be estimated from several wells in this area to include the lateral heterogeneities. Nonetheless, only one well is available for this inversion test, which could increase the uncertainty for lithology and fluid prediction. Also, due to the limited access to the well-log data, a blind well test, which would strengthen the applicability of this method to characterize the carbonate reservoir, could not be performed. Finally, it is necessary to point out that the uncertainties related to scale change and dispersion effects are not included in this study. Because when the compliant fractures and stiff vuggy pores coexist in the heterogeneous carbonates, velocity dispersion can be induced by an internal pore pressure equilibration that takes place with fluid flowing from the more compliant high-pressure regions to the relatively stiffer low-pressure regions. Besides, patchy saturation in the gas carbonate reservoirs may also contribute velocity dispersion. All those factors should be cautiously calibrated to allow more reliable lithofacies prediction.

CONCLUSIONS

Lithology and fluid prediction from seismic data in Sichuan Basin, southwest China is significantly challenging due to its deep burial depth and substantial heterogeneities. With integration of the geologic information, rock-physics analysis, well-log, and seismic data, we applied a Bayesian inversion approach to predict the posterior probabilities for the defined lithofluid classes. We demonstrate that it is important to perform rock-physics analysis before conducting lithology and fluid prediction, in particular for the heterogeneous carbonate reservoir. Based on our geologic understanding of the reservoir, the rock-physics modeling scheme we used gives physical insight into how the lithofluid classes with different rock properties can be related to their corresponding elastic responses. We conclude that the elastic responses of carbonates can be sensitive to the fluids due to the presences of vuggy-fracture pore system in this reservoir. Bayesian seismic inversion helps to characterize the uncertainty of the extracted seismic attributes. For the studied deep targeted carbonate reservoir, it is found that the density prediction is not reliable with high uncertainty. Therefore, we only use P- and S-wave velocities for lithology and fluid prediction. The posterior probabilities for the four defined lithofacies are mapped in the target zone, which aid the identification of the potential gas-carbonate formation with geologic continuity. The case study also illustrates that the prediction strength is controlled by the uncertainty of the rock-physics likelihood and the accuracy of the seismic inversion results.
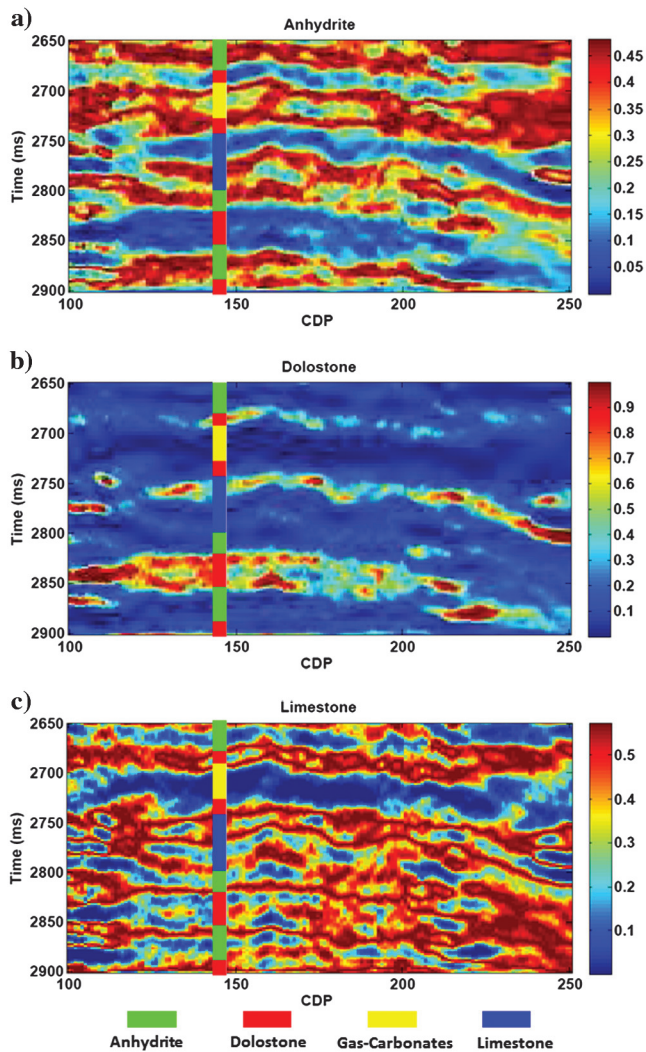
ACKNOWLEDGMENTS

Figure 12. Posterior probabilities for anhydrite, dolostone, and limestone distributions in the targeted reservoir. The corresponding lithofacies profile from well A is plotted for comparison with the inversion results.

REFERENCES

Avseth, P., T. Mukerji, and G. Mavko, 2005, Quantitative seismic interpretation — Applying rock physics tools to reduce interpretation risk: Cambridge University Press.

Bosch, M., T. Mukerji, and E. F. Gonzalez, 2010, Seismic inversion for reservoir properties combining statistical rock physics and geostatistics: A review: Geophysics, **75**, no. 5, A165–A176, doi: 10.1190/1.3478209.

Buland, A., O. Kolbjørnsen, R. Hauge, Ø. Skjæveland, and K. Duffaut, 2008, Bayesian lithology and fluid prediction from seismic prestack data: Geophysics, **73**, no. 3, C13–C21, doi: 10.1190/1.2842150.

Buland, A., and H. Omre, 2003, Bayesian linearized AVO inversion: Geophysics, **68**, 185–198, doi: 10.1190/1.1543206.

Domenico, S. N., 1976, Effect of brine-gas mixture on velocity in an unconsolidated reservoir: Geophysics, **41**, 882–894, doi: 10.1190/1.1440670.

Eidsvik, J., P. Avseth, H. Omre, T. Mukerji, and G. Mavko, 2004, Stochastic reservoir characterization using prestack seismic data: Geophysics, **69**, 978–993, doi: 10.1190/1.1778241.

González, E. F., T. Mukerji, and G. Mavko, 2008, Seismic inversion combining rock physics and multiple-point geostatistics: Geophysics, **73**, no. 1, R11–R21, doi: 10.1190/1.2803748.

Grana, D., and E. D. Rossa, 2010, Probabilistic petrophysical-properties estimation integrating statistical rock physics with seismic inversion: Geophysics, **75**, no. 3, O21–O37, doi: 10.1190/1.3386676.

Gunning, J., and M. E. Glinsky, 2007, Detection of reservoir quality using Bayesian seismic inversion: Geophysics, **72**, no. 3, R37–R49, doi: 10.1190/1.2713043.

Han, D., 2004, Velocity of carbonate rocks: 2004 Annual Report of Fluids: DHI Consortium.

Houck, R. T., 2002, Quantifying the uncertainty in an AVO interpretation: Geophysics, **67**, 117–125, doi: 10.1190/1.1451395.

Hudson, J. A., 1981, Wave speeds and attenuation of elastic waves in material containing cracks: Geophysical Journal of the Royal Astronomical Society, **64**, 133–150, doi: 10.1111/j.1365-246X.1981.tb02662.x.

Larsen, A. L., M. Ulvmoen, H. Omre, and A. Buland, 2006, Bayesian lithology/fluid prediction and simulation on the basis of a Markov-chain prior model: Geophysics, **71**, no. 5, R69–R78, doi: 10.1190/1.2245469.

Li, Y. Y., J. Downton, and B. Goodway, 2003, Recent applications of AVO to carbonate reservoirs in the Western Canadian Sedimentary Basin: The Leading Edge, **22**, 670–674, doi: 10.1190/1.1599694.

Long, R., R. Huang, H. Li, Y. You, G. Liu, and Z. Bai, 2011, Formation mechanism of the Changxing formation gas reservoir in the Yuanba gas field, Sichuan Basin, China: Acta Geologica Sinica, **85**, no. 1, 233–242, doi: 10.1111/j.1755-6724.2011.00393.x.

Lucia, F. J., 1999, Carbonate reservoir characterization: Springer-Verlagnica.

Ma, Y., T. Guo, X. Zhao, and X. Cai, 2008a, The formation mechanism of high-quality dolomite reservoir in the deep of Puguang Gas Field: Science in China Series D: Earth Sciences, **51**, 53–64, doi: 10.1007/s11430-008-5008-y.

Ma, Y., S. Zhang, T. Guo, G. Zhu, X. Cai, and M. Li, 2008b, Petroleum geology of the Puguang sour gas field in the Sichuan Basin, SW China: Marine and Petroleum Geology, **25**, 357–370, doi: 10.1016/j.marpetgeo.2008.01.010.

Mavko, G., T. Mukerji, and J. Dvorkin, 2009, The rock physics handbook: Tools for seismic analysis in porous media: Cambridge University Press.

Mukerji, T., A. Jørstad, P. Avseth, G. Mavko, and J. R. Granli, 2001, Mapping lithofacies and pore-fluid probabilities in a North Sea reservoir: Seismic inversions and statistical rock physics: Geophysics, **66**, 988–1001, doi: 10.1190/1.1487078.

Rimstad, K., P. Avseth, and H. Omre, 2012, Hierarchical Bayesian lithology/fluid prediction: A North Sea case study: Geophysics, **77**, no 2, B69–B85, doi: 10.1190/geo2011-0202.1.

Rimstad, K., and H. Omre, 2010, Impact of rock-physics depth trends and Markov random fields on hierarchical Bayesian lithology/fluid prediction: Geophysics, **75**, no. 4, R93–R108, doi: 10.1190/1.3463475.

Schoenberg, M., and C. M. Sayers, 1995, Seismic anisotropy of fractured rock: Geophysics, **60**, 204–211, doi: 10.1190/1.1443748.

Tarantola, A., 1987, Inverse problem theory and model parameter estimation: Elsevier Science Publishers.

Ulvmoen, M., H. Omre, and A. Buland, 2010, Improved resolution in Bayesian lithology/fluid inversion from prestack seismic data and well observations: Part 1 — Methodology: Geophysics, **75**, no. 2, R21–R35, doi: 10.1190/1.3294570.

Xu, S., and M. A. Payne, 2009, Modeling elastic properties in carbonate rocks: The Leading Edge, **28**, 66–74, doi: 10.1190/1.3064148.

Zhao, L., M. Nasser, and D. Han, 2013, Quantitative geophysical pore type characterization and geological implications in carbonate reservoir: Geophysical Prospecting, **61**, 827–841, doi: 10.1111/1365-2478.12043.